First-principles approach to rotational-vibrational frequencies and infrared intensity for H_{2} adsorbed in nanoporous materials

Lingzhu Kong, Yves J. Chabal, and David C. Langreth

Phys. Rev. B **83**, 121402 — Published 3 March 2011

DOI: 10.1103/PhysRevB.83.121402

First-principles approach to rotational-vibrational frequencies and infrared intensity for H_2 adsorbed in nanoporous materials

Lingzhu Kong,[1] Yves J. Chabal,[2] and David C. Langreth[1]

[1]*Dept. of Physics & Astronomy, Rutgers University, Piscataway, NJ 08854, USA*
[2]*Dept. of Materials Science & Engineering, University of Texas at Dallas, Richardson, TX 75080, USA*

(ΩDated: January 11, 2011)

The absorption sites and the low-lying rotational and vibrational (RV) energy states for H_2 adsorbed within a metal-organic framework are calculated via van der Waals density functional theory. The induced dipole due to bond stretching is found to be accurately given by a first-principles driven approximation using maximally-localized-Wannier-function analysis. The strengths and positions of lines in the complex spectra of RV transitions are in reasonable agreement with experiment, and in particular explain the experimentally mysteriously missing primary line for para hydrogen.

PACS numbers: 68.43.Bc, 78.30.-j, 82.75.-z

Gas adsorption into nanoporous materials is of great interest for both fundamental science and applications. Molecular H_2 is challenging because it can vibrate, rotate, and translate quantum mechanically about its binding site due to its small mass. The vibration-rotation (RV) excitations induced by infrared (IR) absorption thus provide rich information[1]. However, determining the origin and strength of these lines is challenging because large unit cells are encountered in typical nanoporous structures, and the dynamic dipole is distributed over spatially remote parts of the structure. To determine the absorption intensity, a precisely tractable experimental quantity, one must not only calculate the dipole, but also evaluate the quantum mechanical matrix element. An effective approximation scheme for doing this has not hitherto been found.

Here, we present such a scheme based on the combination of a self-consistent van der Waals density functional (vdW-DF) approach[2] with maximally-localized-Wannier-function (MLWF) analysis[3,4] and apply it to H_2 adsorption in a prototypical metal-organic framework, MOF-5[5]. Such materials have been extensively explored for hydrogen storage[6], gas separation, catalysis, and sensors[7]. We analyze the dynamical properties of the adsorbed H_2, finding results consistent with experiment. Importantly, we apply the MLWF analysis to calculate the induced dipole moment due to H_2 adsorption and bond stretching, decomposing the dipole into the contributions from both adsorbed dihydrogen and MOF. Monitoring the change in each Wannier center of the MOF structure upon H_2 adsorption provides an intuitive picture by breaking the H_2-sorbent interaction into individual components of the MOF structure, thus identifying the parts that directly interact with the dihydrogen. Such knowledge is important to optimize MOF structures for desired properties. Here, we use this information to calculate the dynamical dipole moment and its matrix element for H_2 vibrational transitions and RV transitions. We find that the IR intensity of the purely vibrational mode for para-H_2 is only about 2.5% of that for ortho-H_2 at the primary adsorption site, which agrees beautifully with the missing line in the experiment.[8]. A selection rule for RV transitions at the relevant site is also obtained and supported by the IR data.

The H_2 binding sites are efficiently determined by self-consistent vdW-DF calculations[2]. A series of total energy calculations for different bond lengths, orientations, and center-of-mass positions respectively are performed. The resulting potential energy surfaces are then used in the corresponding radial and rigid rotor Schrödinger equations respectively to extract the vibrational, rotational and translational frequencies[9,10]. The rotation-translation coupling is not included. Bacic et al., for example, showed by force-field calculations that this coupling leads to $\sim$2 cm^{-1} difference in the rotational splittings for low-lying states for H_2 in open-cage fullerene[11]. We used the experimental positions for MOF atoms[12,13]. We have checked the effects of optimizing the MOF atoms by relaxing the adsorbed H_2 at cup site together with the nearby MOF atoms $(OZn_3)(CO_2)_3$, which shows that the stretch frequency of H_2 changes by -5 cm^{-1}, bringing it in even better agreement with experiments.

It has been shown that the sum of the Wannier-function centers is connected to the Berry phase theory of bulk polarization[4]. The dipole in the unit cell is given by $\mathbf{u} = e\sum_m Z_m \mathbf{R}_m - e\sum_{n,spin} \mathbf{r}_n$, where Z_m and $\mathbf{R}_m$ are the atomic number and position of the m^{th} nuclei and $\mathbf{r}_n$ is the center of the n^{th} Wannier function. Importantly, it is trivial to decompose the total dipole into components in various parts of the structure[3], which goes beyond the Berry-phase method. Thereby, we may use the change of Wannier center upon adsorption as a qualitative measure for understanding the H_2-MOF interaction and to determine the important parts of the MOF that directly interact with hydrogen.

There are four types of adsorption sites in this structure, as established experimentally[13] and theoretically[14], with reasonable agreement. We start with the positions determined by neutron scattering[13] and relax the H_2 with the vdW-DF approach, thereby confirming the positions of the four sites, named the cup, O3, O2, and benzene sites[13]. Fig. 1 shows the position of the cup site and

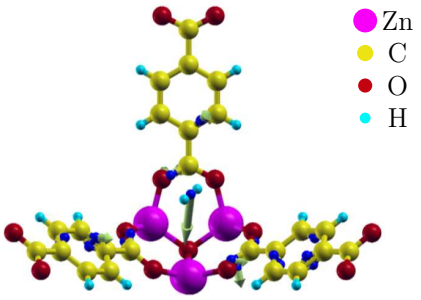

FIG. 1: The primary adsorption site and the change of Wannier centers (blue balls) due to H_2 adsorption compared to bare MOF and free H_2. Vector lengths are enlarged by 1200. The structure shown is just a fraction of the unit cell.

a portion of the MOF-5 structure where there exists 3-fold rotation symmetry among the three benzene ring branches. The distance between the H_2 center-of-mass position and the oxygen atom passing through the rotation axis is about 4.2Å which is somewhat larger than the measured value of 3.8Å[13] due to a known vdW-DF overestimation of bond lengths[15]. Fig. 1 also shows the shift of the Wannier centers upon H_2 adsorption with respect to the bare MOF and the free H_2. See Supplemental Material for other sites[23]. These figures show that the Wannier centers associated with the π bonds in the benzene ring change significantly upon H_2 adsorption for all four adsorption sites, showing a clear and intuitive picture of the MOF components that interact directly with the adsorbed H_2.

Table I shows both the theoretical and experimental stretch frequency shifts of the adsorbed H_2 with respect to the corresponding free H_2 value. The agreement is reasonable. Importantly, the origin of the IR peaks at -19 and -17 cm^{-1} (not understood experimentally[8]) is unraveled here. The calculated binding energies at O2 and O3 sites are very close. However, vdW-DF typically overestimates intermediate-range interactions[16]. Since O3 has three benzene neighbors while O2 has two, the overestimation for the O3 site is expected to be larger than that for the O2 site. As a result, the O2 site is probably more favorable energetically and should get populated more than the O3 site. This is consistent with the measurements where the -17 cm^{-1} peak is quite weak and appears only as a shoulder to the main line at -19 cm^{-1}. We therefore assign the -19 cm^{-1} peak to the O2 site whereas -17 cm^{-1} to O3. The frequency shift of -49 cm^{-1} measured by IR absorption for H_2 at the primary site[17] differs substantially from the -27.5 cm^{-1} reported in Ref. 8, as expected since the differing synthesis methods used in these two reports yield substantially different crystal structures[18]. The standard simple cubic form, measured in Ref. 8, was used for our calculations. Another calculation[14] for this structure obtained a much larger frequency shift in disagreement with the experiment on this structure[8]."

TABLE I: Theory vs experiment[8] for the stretch frequency shift of the adsorbed H_2 relative to free H_2. See text for zero point energies (not included in the binding energies E_B here).

site	Theory (cm^{-1})	Expr. (cm^{-1})	Calculated E_B (kJ/mol)
cup	-23	-27.5	-11.1
O2	-22	-19.0	-7.9
O3	-13	-17	-7.8
benzene	-15	—	-5.4

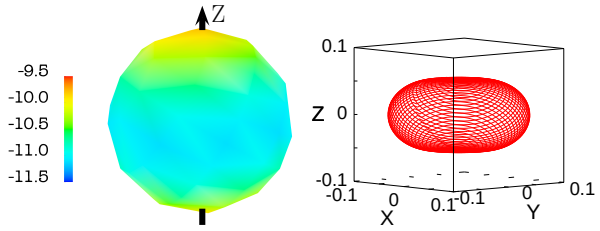

FIG. 2: left: Orientational dependence of the binding energy (kJ/mol) at the cup site; right: Ground state $|\psi_{rot}|^2$. The distance from the origin is the probability for that orientation.

Now consider the RV lines where both vibrational and rotational states change[8]. The left panel of Fig. 2 is the angular potential energy surface at the cup site. The coordinate system is chosen so that the origin is at the cup site and the Z axis is the 3-fold rotation axis (see Fig. S2 in Supplemental Material [23]). Fig. 2 shows that H_2 tends to lie in the XY plane and to be perpendicular to the rotation axis (Z). The energies for in-plane orientations are almost uniform. Therefore, the rotation is essentially two dimensional, as shown by the flattened ground-state angular wave function in the right panel of Fig. 2. Combining the stretch frequency and the rotational energies (see Supplemental Material), we obtain the RV frequencies. The results for the cup site are shown as S transitions in Table II, where the frequency shifts are listed relative to the corresponding free H_2 values (see Supplemental Material for other sites). The magnitude of the shifts is consistent between theory and experiment, particularly for the leading peaks in each category that are most intense.

We also calculated the translational frequencies at the cup site associated with the motion of the whole H_2 against the adsorption site. The three translational frequencies, at 95, 108 and 133 cm^{-1} respectively, are consistent with the value of 84 cm^{-1} extracted from IR spectra[8]. They are also similar to that observed for H_2 in C_{60} (110 cm^{-1})[19]. The determination of the rotational and translational states gives the corresponding zero point energies of $\sim$0.5 and 2 kJ/mol for H_2 at the cup site. The binding energy after corrections is therefore about 8.5 kJ/mol and somewhat larger than the measured adsorption enthalpy of $\sim$5 kJ/mol[20,21]. This overestimation by vdW-DF, also found in other MOF materials[9], is attributed to overestimation of the intermediate-range

interactions[16].

The measured IR spectra for the cup adsorption site shows a strong pure vibrational peak due to the ortho-H_2, while the corresponding para line is not observed. Since the orientational energy map only shows a small rotational barrier, the missing para-H_2 line cannot be explained by the assumption of a frozen H_2 orientation. Moreover, the local structure around this site has C_{3v} symmetry. The rotational state of the para H_2 has the same symmetry as Z and transforms as $A1$. Therefore the transitions between two $A1$ states should be IR active, even though the X and Y components of the dipole give a vanishing contribution by symmetry.

To understand the unexpected missing para-H_2 line and to calculate the line weights in the more complex RV spectra, we evaluate the transition dipole integral explicitly. Assuming the electronic state remains in the ground state and the RV wave function is separable, one has $I_\alpha = \langle\psi^f_{vib}\psi^f_{rot}|u_\alpha|\psi^i_{vib}\psi^i_{rot}\rangle$, where u is the dipole moment and $\alpha = X, Y$, or Z; the translational motion associated with H_2 center-of-mass is not included. The dipole is a function of the H_2 internuclear distance, R, and the bond orientation is defined by (θ, ϕ). It can be expanded as $u_\alpha(R,\theta,\phi) = u_\alpha(R_0,\theta,\phi) + u'_\alpha(R,\theta,\phi)|_{R_0}\,\Delta R$ where R_0 is the equilibrium bond length, and u'_α is the derivative of u_α with respect to R. Since the vibrational wave functions depend only on the inter-nuclear distance, the integral of the first term vanishes for transitions between different vibrational states due to orthogonality. We find $I_\alpha = \langle\psi^f_{vib}|\Delta R|\psi^i_{vib}\rangle\langle\psi^f_{rot}|u'_\alpha(R_0,\theta,\phi)|\psi^i_{rot}\rangle$, where $|\psi^i_{rot}\rangle \equiv |j_i m_i\rangle$ with j even (odd) for para (ortho) H_2, and similarly for $|\psi^f_{rot}\rangle$. The radial integral is a constant for both ortho and para H_2 and therefore unnecessary for understanding the missing line of para-H_2. The angular integral determines the relative intensity between them. We now need to evaluate this integral, for which $u'_\alpha(R_0,\theta,\phi)$ remains to be calculated.

To perform *ab initio* calculations for u'_α for every (θ,ϕ) is computationally expensive and impractical for this system. A possible approach is to compute the dipole from first principles for a few H_2 orientations and derive from them the dipole of all the other orientations. This becomes feasible if one can write the dipole as

$$u_\alpha = \sum\nolimits_i C_{i,\alpha} F_{i,\alpha}(\theta,\phi) \qquad (1)$$

where F are some known functions and the summation needs to be run over only a few terms. This approach is appropriate if one realizes that H_2 and MOF are weakly interacting and the dipole induced on each other can be well described within a classical picture. First, MOF atoms produce an electric field ($\vec{E}$) which induces a dipole on H_2. At the cup site, the field is along Z due to the rotational symmetry so it can be easily shown that the induced dipole on H_2 is of the form in Eq. (1) by projecting the field perpendicular and parallel to the H_2 bond and calculating the corresponding dipole components. A second contribution to the total dipole of the system arises from the H_2 permanent quadrupole inducing a dipole on the MOF. The quadrupolar potential and the corresponding electric field at position $\mathbf{r}$, depend on $\mathbf{r}$, the H_2 quadrupole and the bond orientation, which are again of the form in Eq. (1). This field shifts the MOF charge density and induces a dipole. The total dipole on the MOF may be formally calculated by multiplying the electric field by the polarizability at the same position and integrating over the whole MOF. This procedure extends the classical picture of point charge into the continuous charge density regime. It cannot be performed in practice since the polarizability is not available. However, the final result for the dipole would be like the expression in Eq. (1), since the integration runs over the MOF space while (θ,ϕ) would be left unchanged. One can similarly add second-order corrections where the induced dipole on H_2 and MOF further produce dipole on each other. The final equation after this correction turns out to be quite simple for cup site absorption (see the Supplemental Material for derivation) and reads

$$\begin{aligned} u^s_X &= C^s_1 \sin 2\theta\cos\phi - (C^s_2\cos 2\phi - C^s_3 \sin 2\phi)\sin^2\theta \\ u^s_Y &= C^s_1 \sin 2\theta\sin\phi + (C^s_2\sin 2\phi + C^s_3 \cos 2\phi)\sin^2\theta \\ u^s_Z &= C^s_4\cos^2\theta + C^s_5, \end{aligned} \qquad (2)$$

where s could be H_2, MOF, or the total system. The C's depend on the H_2 quadrupole, polarizability and MOF geometry which are kept fixed during the vibrational transition. Eq. (2) implies that only 2 orientations (each orientation gives 3 equations) are required to determine the five constants and correspondingly the dipole for any other orientations. To test this model, we calculate u'_Z for several H_2 orientations. Good linearity is obtained between u'_Z and $\cos^2\theta$ (see Fig. S7 in Supplemental Material), in agreement with our model. X and Y components are also consistent (see Supplemental Material).

Table II summarizes our results for H_2 at the cup site. First we consider pure vibrations where rotational quantum numbers do not change (the Q lines in Table II). The angular integral (I^2_A) for Q(0) (para) is much smaller than that for Q(1) (ortho), owing partly to the vanishing of the X and Y components of the dipole for the Q(0) transition due to symmetry. This symmetry issue also applies to the $|jm>= |10\rangle\rightarrow|10\rangle$ transition in Q(1) so that the integral is about 1/3 of that for the other two transitions of Q(1). Additionally, Fig. 2 shows that para H_2 has a larger probability to be oriented in XY plane, giving a smaller u'_Z upon bond stretching, while the $|10\rangle$ state of ortho H_2 is p_z like and the H_2 bond is mainly perpendicular to XY plane. As a result, u'^2_Z for the para state is only about one quarter of that for the $|10\rangle$ state (see Supplemental Material for the integral results of each component of $\mathbf{u}'$ for the Q transitions). To get the relative intensity between Q(0) and Q(1), we need to consider the population ratio between para and ortho hydrogen, which we took to be 1:3. Also, the calculated rotational energy of the $|10\rangle$ state is about 5.5 meV higher than that for the $m = \pm 1$ states (see Supplemental Material).

TABLE II: Theory vs. experiment[8] for RV transitions at the cup site. The frequency shift Δv (cm^{-1}) is relative to the corresponding free H_2 value. The theoretical intensity [$\propto I_\alpha^2$ times the 30K Boltzmann factor (times 3 for ortho)] is normalized to 100 for the strongest line; strong (str), weak (wk), and absent (abs) describe the experimental intensity.

	m_i	m_f	Theory		Experiment	
			Δv	Int.	Δv	Int.
Q(0)	0	0	−23	2		abs
Q(1)	±1	±1	−23	97	−27.5	str
	0	0				
Q*(1)	±1	0	22	9	39	wk
S(0)	0	±2	−44	58	−49.3	str
		±1	−12	5	−6.8	wk
		0	−1	2		abs
S(1)	±1	±3	−34	100	−36.8	str
		±2	−9	6	−0.8	wk
		±1	6	9	21.6	wk
		0	11	3		abs
	0	±3	−78	0		abs
		±2	−53	3	−61	wk
		±1	−50	∼0		abs
		0	−33	∼0		abs

As such, its population is about 13% of that of the $m = 1$ or -1 state at the experimental $T = 30$K within a Boltzmann distribution. We can therefore estimate that the vibrational intensity for para H_2 is about 2.5% of that for ortho H_2, hence agreeing with the IR measurement, where the para line was simply not observed[8].

Table II also shows the results for S lines in the IR spectrum, where $\Delta j = 2$. First a selection rule of $\Delta m = \pm 2$ is observed with small probabilities for other transitions. This table also predicts one single strong line for each S(0) and S(1) at the experimental $T = 30$K, with shifts of -44 and -34 cm^{-1} respectively, whereas the S(1) line at -53 cm^{-1} should be weak due to the low population of the $|10\rangle$ state. More importantly, the strong line in each category exhibits the largest frequency relative to the free H_2 value, agreeing very well with Ref. 8, where a single strong S(0) line of -49.3 cm^{-1} and a strong S(1) line of -36.8 cm^{-1} are observed for H_2 at the cup site. A weak S(0) line at -6.8 cm^{-1} and two S(1) peaks at -0.8 and 21.6 cm^{-1} are also observed with intensities roughly one order of magnitude smaller than that of the corresponding strong line, consistent with our calculations. Furthermore, Table II shows that the calculated intensities of the two strong S lines and the Q(1) lines are comparable, which is also observed[22]. We also note a peak of ~ -61 cm^{-1} shift with an intensity similar to that of the S(1) at -0.8 cm^{-1}[22]. This peak might arise from the $|10\rangle \rightarrow |3, \pm 2\rangle$ transitions with theoretical intensity close to those of the other two weak S(1) lines, after the 13% population weight is taken into account(Table II). Finally, we discuss the special Q*(1) line ($|1, \pm 1\rangle \rightarrow |10\rangle$) that is experimentally observed[8]. The calculated I_A^2 of this transition is approximately equal to that for Q(0). However, the para:ortho ratio is ∼1:3 which makes Q*(1) 3∼4 times stronger and observable. The calculated shift of 22 cm^{-1} is quite small compared to the experimental value of 39 cm^{-1}. This is likely due to the neglect of rotation-translation coupling, which would probably lower the low rotational state even more and therefore increase the splitting between the m=0 and m=±1 states.

In summary, we have proposed a method that provides an intuitive picture of H_2 interaction in complex environments. These techniques provide powerful tools for studying gas adsorption in general.

Supported by DOE Grant No. DE-FG02-08ER46491.

[1] Y. J. Chabal and C. K. N. Patel, Phys. Rev. Lett. **53**, 210 (1984).

[2] M. Dion et al., Phys. Rev. Lett. **92**, 246401 (2005); T. Thonhauser et al., Phys. Rev. B **76**, 125112 (2007); G. Román-Pérez and J. Soler, Phys. Rev. Lett. **103**, 096102 (2009).

[3] N. Marzari and D. Vanderbilt, Phys. Rev. B, **56**, 12847 (1997); I. Souza et al., Phys. Rev. B, **62**, 15505 (2000).

[4] R. D. King-Smith and D. Vanderbilt, Phys. Rev. B **47**, 1651 (1993).

[5] N. L. Rosi *et al.*, Science **300**, 1127 (2003).

[6] L. J. Murray, M. Dincă, and J. R. Long, Chem. Soc. Rev. **38**, 1294 (2009).

[7] A. U. Czaja, N. Trukhan, and U. Müller, Chem. Soc. Rev. **38**, 1284 (2009).

[8] S. A. FitzGerald *et al.*, Phys. Rev. B **77**, 224301 (2008).

[9] L. Kong *et al.*, Phys. Rev. B **79**, 081407 (2009).

[10] L. Kong, G. Román-Pérez, J. M. Soler, and D. C. Langreth, Phys. Rev. Lett. **103**, 096103 (2009).

[11] S. Ye *et al.*, J. Phys. Chem. A **114**, 9936 (2010).

[12] J. L. C. Rowsell *et al.*, Science **309**, 1350 (2005).

[13] T. Yildirim and M. R. Hartman, Phys. Rev. Lett. **95**, 215504 (2005).

[14] K. Sillar, A. Hofmann, and J. Sauer, J. Am. Chem. Soc. **131**, 4143 (2009).

[15] D. C. Langreth *et al.*, J. Phys.: Cond. Mat. **21**, 084203 (2009).

[16] K. Lee *et al.*, Phys. Rev. B **82**, 081101 (2010).

[17] S. Bordiga *et al.*, J. Phys. Chem. B **109**, 18237 (2005).

[18] J. Hafizovic *et al.*, J. Am. Chem. Soc. **129**, 3612 (2007).

[19] S. A. FitzGerald, S. Forth, and M. Rinkoski, Phys. Rev. B **65**, 140302 (2002).

[20] J. L. C. Rowsell and O. M. Yaghi, J. Am. Chem. Soc. **128**, 1304 (2006).

[21] S. S. Kaye and J. R. Long, J. Am. Chem. Soc. **127**, 6506 (2005).

[22] S. A. FitzGerald *et al.*, Phys. Rev. B **81**, 104305 (2010).

[23] See Supplemental Material at http://link.aps.org/ supplemental/10.1103/PhysRevLett.000.000000.